Korean Journal of Radiology

Trastuzumab-Conjugated Liposome-Coated Fluorescent Magnetic Nanoparticles to Target Breast Cancer

Mijung Jang, MD[1], Young Il Yoon, MS[2], Yong Soo Kwon, MS[3], Tae-Jong Yoon, PhD[2, 3], Hak Jong Lee, MD[1, 2, 4], Sung Il Hwang, MD[1], Bo La Yun, MD[1], Sun Mi Kim, MD[1]

[1]Department of Radiology, Seoul National University Bundang Hospital, Seongnam 463-707, Korea; [2]Nanoimaging and Therapy Research Center, Institute of Nanoconvergence, Advanced Institutes of Convergence Technology, Seoul National University, Suwon 443-270, Korea; [3]NanoBio Materials Chemistry Lab., Department of Applied Bioscience, CHA University, Pocheon 487-010, Korea; [4]Program in Nano Science and Technology, Department of Transdisciplinary Studies, Seoul National University Graduate School of Convergence Science and Technology, Suwon 443-270, Korea

Objective: To synthesize mesoporous silica-core-shell magnetic nanoparticles (MNPs) encapsulated by liposomes (Lipo [MNP@m-SiO$_2$]) in order to enhance their stability, allow them to be used in any buffer solution, and to produce trastuzumab-conjugated (Lipo[MNP@m-SiO$_2$]-Her2$_{Ab}$) nanoparticles to be utilized *in vitro* for the targeting of breast cancer.

Materials and Methods: The physiochemical characteristics of Lipo[MNP@m-SiO$_2$] were assessed in terms of size, morphological features, and *in vitro* safety. The multimodal imaging properties of the organic dye incorporated into Lipo[MNP@m-SiO$_2$] were assessed with both *in vitro* fluorescence and MR imaging. The specific targeting ability of trastuzumab (Her2/*neu* antibody, Herceptin®)-conjugated Lipo[MNP@m-SiO$_2$] for Her2/*neu*-positive breast cancer cells was also evaluated with fluorescence and MR imaging.

Results: We obtained uniformly-sized and evenly distributed Lipo[MNP@m-SiO$_2$] that demonstrated biological stability, while not disrupting cell viability. Her2/*neu*-positive breast cancer cell targeting by trastuzumab-conjugated Lipo[MNP@ m-SiO$_2$] was observed by *in vitro* fluorescence and MR imaging.

Conclusion: Trastuzumab-conjugated Lipo[MNP@m-SiO$_2$] is a potential treatment tool for targeted drug delivery in Her2/ *neu*-positive breast cancer.

Index terms: *Breast cancer; Drug delivery; Iron oxide nanoparticles; Magnetic resonance imaging; Trastuzumab*

INTRODUCTION

Nanotechnology has been increasingly leveraged in cancer research, particularly for the development of novel detection and treatment options (1). Magnetic nanoparticles (MNPs), composed of a magnetic core (e.g., iron oxide) and biocompatible polymeric shell, offers a particularly attractive delivery option for biomarker-targeted magnetic resonance imaging (MRI) contrast agents and drug treatments. Indeed, MNPs have been widely used for myriad *in vitro* and *in vivo* applications, such as MRI

contrast enhancement, immunoassays, and drug delivery (2-6). These applications require the MNPs to have special characteristics, such as high magnetization, small size, narrow-size distribution, and specialized surface coating, which allow targetable delivery to specific areas (4). Recently, these multifunctional nanostructured materials have been applied to multimodal imaging and simultaneous diagnosis and therapy (7).

The nanoparticle coating material serves a particularly important role as it can be adjusted to change its therapeutic properties. Silica is considered a good coating material because of its biocompatibility and resistance to biodegradation, while also being a useful delivery vehicle because of its uniform pore size, large surface area, and highly accessible pore volume (8). Moreover, silica is stable in aqueous-based solutions and has a high labeling efficiency making it an excellent candidate for use *in vivo* (7, 9-11). Finally, using liposomes to encapsulate the coated nanoparticles is a well-established method that results in stable *in vivo* behavior in conjunction with a long circulation time. Liposomes can also contain a large number of MNP cores and can, therefore, deliver them undiluted, to the target site (12).

In order to increase selectivity and recognition, antibodies targeting cancer cells can be modified and secured onto the liposome encapsulated nanoparticles. One such ligand, receptor 2 (Her2), has been utilized for this technique. Although Her2/*neu* is expressed at low levels in normal adult tissues, it is upregulated in approximately 30% of breast cancers and 20% of ovarian cancers (13, 14). Trastuzumab (Her2/*neu* expression receptor antibody, Herceptin®, Genentech, Inc., South San Francisco, CA, USA) is a humanized monoclonal antibody against Her2/*neu* that is currently being used to treat Her2/*neu*-positive breast cancers (15). The usage of trastuzumab and the mechanism underlying its biological effects have been reviewed extensively (16, 17). The conjugation of trastuzumab to an encapsulated nanoparticle would allow for the transport of this targeted therapeutic agent specifically to Her2/*neu*-positive breast cancer cells.

The two main purposes of this study were to: 1) synthesize mesoporous silica-core-shell MNPs encapsulated by liposomes (Lipo[MNP@*m*-SiO$_2$]) in order to enhance their stability, allowing them to be used in any buffer solution; 2) produce trastuzumab-conjugated (Lipo[MNP@*m*-SiO$_2$]-Her2$_{Ab}$) nanoparticles to be utilized *in vitro* that could target breast cancer.

MATERIALS AND METHODS

Chemicals

Iron (III) acetylacetonate [Fe(acac)$_3$, 99.9%], iron (II) acetylacetonate [Fe(acac)$_2$, 99.95%], 1,2-hexadecandiol (90%), oleic acid (OA, 99%), oleylamine (OY, 70%), 1-octadecene (ODE, 95%), chloroform (99%), dimethyl sulfoxide (99.9%), and N-hydroxysulfosuccinimide sodium salt (98.5%) were purchased from Sigma-Aldrich, and used without further modifications. The lipid chemicals were purchased from Avanti Polar Lipids Inc. (Alabaster, AL, USA). Isopropanol (99.5%), hexane (98.5%), ethanol (99.5%), and NaHCO$_3$ were purchased from Fisher Scientific, Korea Ltd., and used without further purification.

Synthesis of MNP@*m*-SiO$_2$

We first synthesized 10 nm Mn-MNPs as seeds for subsequent particle growth as described previously (18). Briefly, Fe(acac)$_3$ (4 mmol, 1.4 g), Fe(acac)$_2$ (2 mmol, 0.5 g), 1,2-hexadecanediol (10 mmol, 2.9 g), OA (6 mmol, 1.9 mL), OY (6 mmol, 2.8 mL), and ODE (20 mL) were mixed by stirring under a steady flow of nitrogen gas for one hour. The combined mixture was heated and kept at a temperature of 200°C for 2 hours. The temperature was then quickly raised to 280°C to initiate particle formation. After reflux, the mixture was cooled to room temperature and isopropanol (4 mL) was added. MNPs were collected by centrifugation (1811 x g, 15 minutes), and the precipitates were redispersed in hexane. To produce larger MNPs from the seed particles, 10 nm MNPs (100 mg) were dissolved in hexane (10 mL) with the same amounts of metal acetylacetonates, 1,2-hexadecanediol, OA, OY, and ODE as described above. Under a steady flow of nitrogen gas, the mixture was heated and kept at 100°C for one hour. The temperature was then elevated to 200°C and maintained for two hours. Finally, the mixture was heated again to 300°C and refluxed for two hours before being cooled to room temperature. The 12-nm MNPs were collected using the same washing and isolation procedure as described above. The 16-nm MNPs were prepared in a similar manner, using the 12-nm particles as seeds.

To generate water-soluble MNPs, 600 µL of particle solution was diluted to 2 mg/mL in chloroform (CHCl$_3$) in a 2-neck round-bottom flask, followed by the addition of 5 mL of 0.05 mM hexadecyltrimethylammonium bromide (CTAB) (10). The mixture was vigorously stirred for one hour; the temperature was then increased to 60°C to

remove the organic solvent. After 20 minutes passed, the temperature was lowered to 70°C and 25 mL of distilled water and 1.8 mL of 2 N NaOH were added. Ethyl acetate (1.8 mL) was then stirred into the mixture, followed by the dropwise addition of 0.3 mL of tetraethylorthosilicate (TEOS) over six hours. Subsequently, the mixture was centrifuged for 20 minutes at 14000 rpm and washed separately with ethanol and distilled water. To completely remove CTAB in the product, 0.05 mL of HCl was added; the solution was then vigorously stirred for 30 minutes. The morphological features, structure, composition, and magnetic properties of the resulting 80-nm iron oxide mesoporous silica-core-shell nanoparticles (MNP@m-SiO$_2$) were characterized using a transmission electron microscope (TEM; JEOL 2100, JEOL, Peabody, MA, USA), an X-ray powder diffractometer (XRD; RU300, Rigaku, Kyoto, Japan), an inductively coupled plasma atomic emission spectrometer (ICP-AES; Activa-S, HORIBA Jobin Yvon, Palaiseau, France), and a vibrating sample magnetometer (VSM), respectively (16).

Synthesis of Lipo[MNP@m-SiO$_2$] and Organic Dye Incorporation

1,2-dipalmitory-sn-glycero-3-phosphatidylcholine (20 µmol, 15.4 mg), cholesterol (9 µmol, 3.48 mg), dicetyl phosphate (1.8 µmol, 1 mg), and 1,2-dipalmitory-sn-glycero-3-phosphoethanolamine (DPPE) (1 µmol, 1.1 mg) were dissolved in 5 mL of CHCl$_3$ and stirred homogeneously. After one hour passed, the solvent evaporated; it was then completely removed by freeze-drying in order to generate the lipid film. MNP@m-SiO$_2$ incorporating the green fluorescent organic dye, fluorescein isothiocyanate (FITC) (0.046 mM), which were produced using the typical silicon compound modification method (11), and 2 mL of hydrophilic red fluorescent organic dye (Texas-red [TR], 0.1 mg/mL) were mixed in H$_2$O, added to the dried lipid film, and homogenized for five minutes. To obtain regular-sized nanoparticles, the liposome-coated nanoparticles were filtered using a 0.45-µm membrane syringe. Excess organic dye was washed out with three rounds of centrifugation (13000 rpm, 5 minutes), and the liposome-coated nanoparticles were redispersed in 2 mL of phosphate-buffered saline (PBS) buffer solution.

Trastuzumab (Her2/*neu* Expression Receptor Antibody) Conjugation with Lipo[MNP@m-SiO$_2$]-Her2$_{Ab}$

To conjugate the Lipo[MNP@m-SiO$_2$] Sulfo-succinimidyl-4-(N-maleimidomethyl) cyclohexane-1-carboxylate

(Aldrich, Sulfo-SMCC, 90%), an amide bond was formed from the primary amine of the particle. Overall, the amine-terminated particle (0.05 mM) was dispersed in 2 mL PBS, and then added to Sulfo-SMCC (5 mg). The mixture was stirred for two hours at room temperature. The conjugated nanoparticles were precipitated by centrifugation (13000 rpm, 15 minutes) and washed three times with H$_2$O. To conjugate the Her2/*neu* expression receptor antibody to the nanoparticles, we first thiolated trastuzumab with Traut's reagent according to the Pierce protocol (19). Trastuzumab (Herceptin®, 5 mg) and cysteamine (2-MEA, 10 mg) were dissolved in 2 mL of 10 mM ethylenediaminetetraacetic acid, followed by incubation and shaking for 1.5 hours at 37°C. The thiol-active antibody was purified with a PD-10 desalting column (GE Healthcare Bio-Sciences, Uppsala, Sweden), and immediately combined with 0.05 mL of the maleimide-terminated Lipo[MNP@m-SiO$_2$]. The mixture was shaken for six hours at 4°C and subsequently purified using centrifugation. To verify the efficacy of the trastuzumab-conjugated particles, cetuximab, a monoclonal antibody that inhibits an epidermal growth factor receptor, was also MNP-conjugated and utilized as a negative control.

Cell Culture and Cytotoxicity Assay

Mouse NIH/3T3 fibroblasts were cultured in Dulbecco's Modified Eagle Medium (DMEM H16; Gibco, Grand Island, NY, USA), supplemented with fetal bovine serum (FBS, 10%), penicillin and streptomycin (1%), L-glutamine (1%), and sodium bicarbonate (2%). Human SKBR-3 breast cancer cells were cultured in the vendor-provided DMEM H16 media. Cells were maintained at 37°C in a humidified atmosphere containing 5% CO$_2$. On achieving confluence, the cells were washed, trypsinized, and resuspended in the culture medium. Cells were then seeded at a concentration of 5000 cells/well in a 96-well tissue culture plate and allowed to grow overnight at 37°C under 5% CO$_2$. Different concentrations of the aqueous nanoparticle solution were added into the culture medium, and the cells were allowed to grow for another 24 hours. To confirm whether the uptake of the nanoparticles was mediated by energy-dependent endocytosis (20), the cells were incubated with the particles at 37°C and 4°C.

To test cell viability in the presence of the nanoparticles, the 3-(4,5-dimethylthiazol-2-yl)-2,5-diphenyltetrazolium (MTT) assay kit (Sigma Cat. No. TOX1, *In vitro* Toxicology Assay Kit) was used. After replacing the culture medium with MTT solution and incubating for 3 hours at 37°C

under 5% CO_2, the MTT solubilization solution was added to dissolve the resulting formazan crystals. Cell viability was measured spectrophotometrically at a wavelength of 570 nm, with a background absorbance at 690 nm.
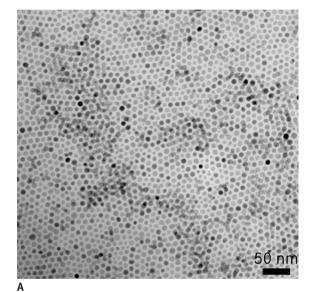
Inductively Coupled Plasma-Atomic Emission Spectroscopy (ICP-AES) Analysis

To accurately measure the metal dose, the mesoporous silica coated MNP was treated with 4% hydrofluoric acid solution and stirred vigorously for 30 minutes. After the solution was brown in color, a 10% HCl solution was added continuously to dissolve MNP core. After stirring for one hour, we observed the color change from brown to yellow in the solution. This acidic solution was then purified using a syringe filter (PTFE 0.2 μm pore) and used for ICP-AES

analysis (Activa-S, HORIBA Jobin Yvon).

In Vitro Magnetic Resonance Imaging

T2-weighted spin-echo MRI was performed with a clinical 3.0-T magnetic resonance scanner (Achieva, Philips Medical System, Best, the Netherland) and SENSE 8 channel wrist coil. For cell imaging, the SKBR-3 breast cancer cell line (2.5×10^5 cells) was incubated with Lipo[MNP@m-SiO$_2$] and Lipo[MNP@m-SiO$_2$]-Her2$_{Ab}$ at a concentration of 10 μg/mL in 10% FBS DMEM for 1 hour at 37°C. After incubation, the cells were washed and pelleted. The cells were then mixed with 2% agarose in PBS, and placed into Eppendorf tubes before being placed in the MR scanner. All samples were scanned with a fast spin-echo pulse sequence with the following parameters: flip angle, 90°; 1 acquisition; field of
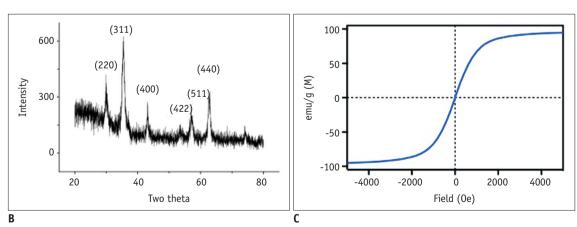
A

B

C

Fig. 1. Structural and magnetic characterization of prepared Fe$_3$O$_4$ magnetic nanoparticles (MNPs).
A. Magnetic nanoparticles obtained by seed-mediated growth had narrow size distribution and consisted of single domain. **B.** X-ray powder diffractogram of 16-nm MNP. MNPs exhibited similar pattern, confirming their ferrite structure and crystal sizes, measured by fitting major peak (311), were in agreement with transmission electron microscopy estimation. **C.** Magnetic properties of MNP determined with vibrating sample magnetometer. Particles were superparamagnetic at 27°C. Relaxivity (r$_2$) was measured at 0.47 T and 40°C. 16-nm MNP showed high r$_2$ of 320 s^{-1}·mM^{-1} (metal).

view, 190 x 80 mm; matrix, 348 x 248; voxel size, 0.60 x 0.75 mm; and slice thickness, 3 mm. Specialized software was used for data acquisition. To estimate the T2 relaxation time

for each sample, axial MR images were acquired at various echo times (TE) from 10 ms to 100 ms with a repetition time 10000 ms. The signal intensities of different slices
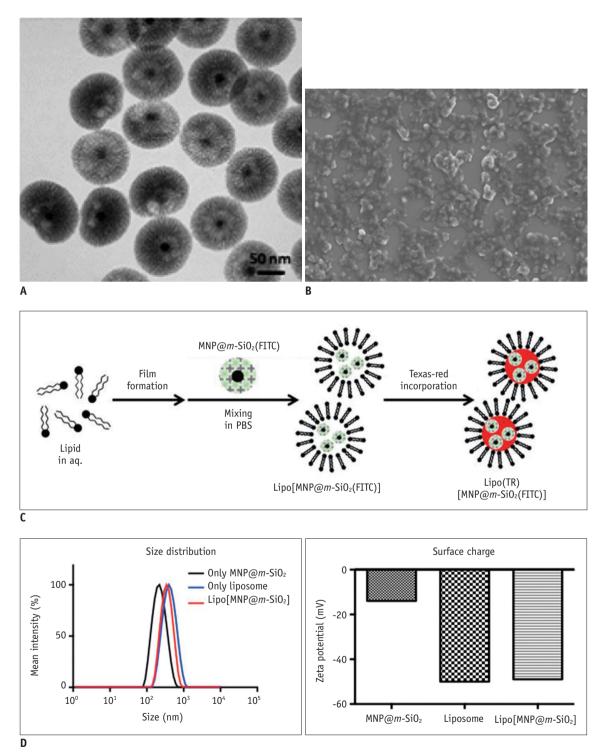

Fig. 2. Synthesis and characterization of Lipo[MNP@m-SiO$_2$] particle.
A. Transmission electron microscopy image of MNP@m-SiO$_2$ particles. Black core dot represents 16-nm Fe$_3$O$_4$ magnetic nanoparticle and wrinkled shell in grey represents m-SiO$_2$. **B.** Scanning electron microscopy image of Lipo[MNP@m-SiO$_2$] showing monodispersed size and shape. **C.** Simple synthetic scheme for Lipo[MNP@m-SiO$_2$]. **D.** Size distribution and surface charge of prepared MNP@m-SiO$_2$, liposome, and Lipo[MNP@m-SiO$_2$] were investigated by dynamic light scattering.

were measured within manually drawn regions of interest (ROIs). Relaxation rates R_2 (R_2 = 1 / T2) were calculated by single-exponential curve fitting of the signal intensity vs. time (TE). The following equation was used for curve fitting (21, 22):

For relaxation rate R_2: $y = A + C*[exp(-R_2*TE)]$

RESULTS

The iron oxide (Fe_3O_4) MNPs (un-coated) utilized during the thermal decomposition seeding process (18) were monitored in regards to: their size, ferrite pattern, and magnetic properties using TEM, p-XRD, and VSM (Fig. 1). The MNPs were found to have the typical inverse-spinel ferrite structure with a monodispersed size distribution. These prepared iron oxide superparamagnetic nanoparticles were used to form the mesoporous silica (m-SiO$_2$)-shell nanoparticles (MNP@m-SiO$_2$) to increase biocompatibility. The shape and size of these coated MNPs were characterized using a TEM and scanning election microscope (Fig. 2A, B). Importantly, the m-SiO$_2$ shell appears to prevent the release of heavy metal ions from the iron oxide core and retain more of the magnetic properties compared to the amorphous silica core shell alone (23). However, the m-SiO$_2$-coated particles (MNP@m-SiO$_2$) did not show long-term solubility in aqueous or buffer solutions.

To produce nanoparticles that were high-stable in a variety of aqueous solutions, we hybridized the m-SiO$_2$-coated particles with liposomes, yielding Lipo[MNP@m-SiO$_2$]. As shown in Figure 2C, a thin film of the liposomes was mixed with the FITC-incorporated MNP@m-SiO$_2$ particle solution, generating the Lipo[MNP@m-SiO$_2$]. To utilize dual fluorescence imaging with green and red colors, TR hydrophilic organic dye was also added. Although the Lipo[MNP@m-SiO$_2$] were slightly larger compared to the liposomes alone, it is unlikely that the incorporation of the dye-labeled MNPs will greatly affect the underlying structure of the 200-nm liposomes. The surface charges of the MNP@m-SiO$_2$, liposomes, and Lipo[MNP@m-SiO$_2$] were measured as -14, -50, and -49 mV, respectively (Fig. 2D).

Furthermore, to investigate the potential use of targeted therapy utilizing these nanoparticles, we conjugated Her2/neu antibodies onto the prepared Lipo(TR)[MNP@m-SiO$_2$(FITC)] (Fig. 3). To determine the cytotoxicity of the prepared particles, normal 3T3 fibroblast and SKBR-3 breast cancer cells were incubated for 24 hours with different amounts of [MNP@m-SiO$_2$], Lipo[MNP@m-SiO$_2$], and Lipo(TR)[MNP@m-SiO$_2$(FITC)]-Her2$_{Ab}$. Cellular viability was then measured using the MTT bromide assay. No acute cytotoxicity was observed, even at a high metal dose (60 µM) for Lipo[MNP@m-SiO$_2$] demonstrating its biocompatibility (Fig. 4). Furthermore, results suggest that Lipo(TR)[MNP@m-SiO$_2$(FITC)]-Her2$_{Ab}$ is able to
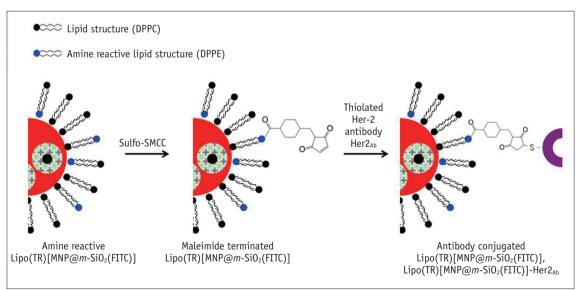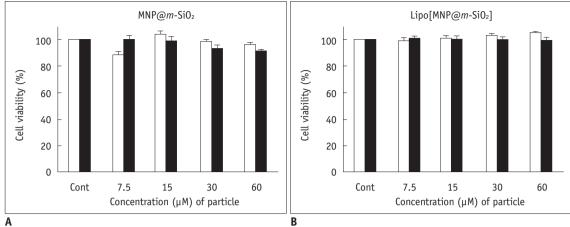

Fig. 3. Synthetic scheme for Her2/neu antibody conjugation onto prepared Lipo(TR)[MNP@m-SiO$_2$(FITC)]. Synthesized Lipo(TR) [MNP@m-SiO$_2$(FITC)] contained active amine site for DPPE lipid during preparatory steps. To terminate maleimide functional group on particle, commercially available Sulfo-SMCC was used and reacted with Lipo(TR)[MNP@m-SiO$_2$(FITC)] by substitution reaction. Maleimide functional group could then be easily attached to thiol group of Her2/neu antibody after inducing thiolation of antibody with Traut's reagent. DPPC = 1,2-dipalmitory-sn-glycero-3-phosphatidycholine, DPPE = 1,2-dipalmitory-sn-glycero-3-phosphoethanolamine, Sulfo-SMCC = Sulfo-succinimidyl-4-(N-maleimidomethyl) cyclohexane-1-carboxylate

Fig. 4. Magnetic nanoparticle cytotoxicity assay.
Normal (3T3 fibroblast, white bar) and cancer (SKBR-3, black bar) cells were incubated for 24 hours in presence of varying amounts of particles. Cellular viability was then measured with 3-(4,5-dimethylthiazol-2-yl)-2,5-diphenyltetrazolium (MTT) bromide assay using [MNP@*m*-SiO$_2$] **(A)** and Lipo[MNP@*m*-SiO$_2$]MNP@ **(B)**.

specifically target SKBR-3 breast cancer cells at different time points during treatment. The fluorophore intensity observed in the cells was completely dependent on the internalized nanoparticles and increased over the course of the treatment. The particles appeared to be dispersed in the cytosol, but were not present in the nucleus. The bare Lipo(TR)[MNP@*m*-SiO$_2$(FITC)] without antibody conjugation was not taken up by the cells after treatment for the following time periods: 1 hour, 3 hours, and 6 hours (Fig. 5A). Importantly, the negative control antibody (cetuximab)-conjugated particles were not taken up by the cells (Fig. 5B), highlighting the specificity of the Her2/*neu* antibody. Furthermore, by altering the incubation temperature for the SKBR-3 cells from 37°C to 4°C, uptake of the MNPs can be significantly impeded, demonstrating that particle uptake into the cells occurs through temperature and time dependent endocytosis (Fig. 5C).
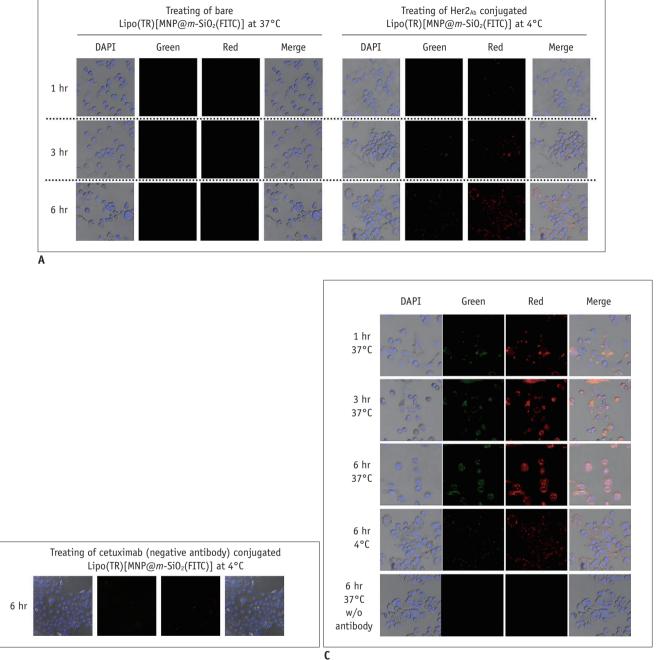
After using Lipo(TR)[MNP@*m*-SiO$_2$(FITC)]-Her2$_{Ab}$ to specifically target SKBR-3 cells, we also observed intense black contrast imaging for the cancer cell pellet using T2-weighted spin-echo MRI (Fig. 6A). When these results were compared with those for non-antibody particle-treated cancer cells, the contrast area showed much lower MR intensity. Typically, superparamagnetic iron oxide particles showed a negative contrast signal in the T2 relaxation time. However, the cell pellet for the treatment with bare particles showed similar contrast intensity to that of cells alone. Further, in the T2 relaxation analysis curves of each cell phantom (Fig. 6B), the Lipo[MNP@*m*-SiO$_2$]-Her2$_{Ab}$-targeted cells showed approximately a 6-fold higher contrast intensity than the control as a result of the pronounced T2

effect, a decrease in signal intensity was observed for the Her2/*neu* targeted cells (Fig. 6C). The mean signal intensity of each cell phantom was significantly different ($p < 0.000$). Thus, Lipo[MNP@*m*-SiO$_2$] has long-term stability in biological solutions, such as buffer or aqueous phases, for at least one month and showed specificity to breast cancer cells after being conjugated to trastuzumab.

DISCUSSION

Given the unique pharmacokinetics of nanoparticles and their large surface area enabling the conjugation of ligands and antibodies, biocompatible MNPs have many advantages in the targeted delivery of therapeutics and imaging agents. Iron oxide in the core of the nanoparticles produces a large magnetic difference between the particle and the surrounding medium, resulting in the generation of microscopic magnetic field gradients and T2 shortening. As a result of the more pronounced T2 and T2* contrast, superparamagnetic nanoparticles are typically used to provide enhanced negative contrast using T2-weighted pulse sequences (12). Indeed, because of their biocompatibility and low toxicity, MNPs have been widely utilized to develop novel biomarker-specific agents. Most notably, these agents have been applied, in conjunction with MRI, for oncologic imaging and detection. Additionally, the detectable changes in the MRI signal produced by the drug-loaded MNPs provide increased imaging capabilities for tracking drug delivery, estimating tissue drug levels, and monitoring therapeutic responses *in vivo*.

Variable synthetic protocols and different combinations

Fig. 5. Specific targeting of breast cancer cells using Her2/*neu* antibody conjugated magnetic nanoparticles (MNPs).
Dual fluorescent imaging using confocal laser scanning microscopy (CLSM) was performed on SKBR-3 breast cancer cells after treatment with bare Lipo(TR)[MNP@*m*-SiO$_2$(FITC)] without antibody conjugation and Lipo(TR)[MNP@*m*-SiO$_2$(FITC)]-Her2$_{Ab}$ **(A)**; negative control Lipo(TR)[MNP@*m*-SiO$_2$(FITC)]-cetuximab **(B)** carrying green and red organic dyes were subjected to fluorescence imaging by using CLSM. Uptake of MNPs through endocytosis was hindered by decreasing incubation temperature for SKBR-3 cells from 37°C to 4°C **(C)**. Green = FITC, Red = hydrophilic regions, Blue = DAPI/nuclei

of coating materials and core shell structure(s) have been investigated for their potential biomedical application. In our study, liposomes with a silica core shell were selected as the delivery system of choice. Liposome encapsulation of MNPs is increasingly being utilized because of the well-established *in vivo* behavior of liposomes, their capacity to hold a large number of nanoparticle cores, and their modifiable surface, which enables more specific cellular targeting properties (12). Further, silica materials also have very flexible intrinsic properties that can be utilized in drug delivery systems (9, 24), such as their stability in aqueous environments and ease of synthesis (12). Mesoporous silica
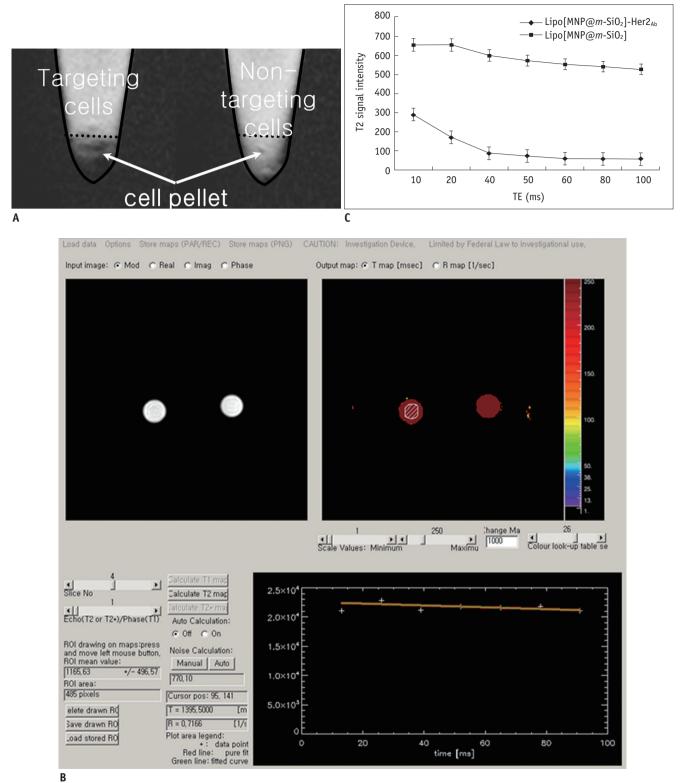
Fig. 6. MR imaging of breast cancer cells after targeting with Lipo[MNP@*m*-SiO₂]-Her2ₐᵦ.
T2 weighted images of SKBR-3 breast cancer cells after treatment with bare (Lipo[MNP@*m*-SiO₂]) and trastuzumab conjugated nanoparticles (Lipo[MNP@*m*-SiO₂]-Her2ₐᵦ) **(A)** T2 relaxometry. T2 weighted images of Lipo[MNP@*m*-SiO₂] with and without trastuzumab conjugation. When regions of interest (ROI) was placed in cell pellet, T2 value can be automatically calculated **(B)**. **(C)** Single-exponential fit of mean signal intensity versus echo time (TE) from Lipo[MNP@*m*-SiO₂] with and without trastuzumab conjugation in different axial slices. Data as mean intensity with ROI with standard deviation in intensities of pixel.

shells are generally regarded as safe and their use, alone or in conjugation with other materials, in diagnostic and biomedical research is increasing (9, 10, 24, 25). However, the long-term toxicity of silica nanoparticles, which are not biodegradable, represents a serious issue for their usability. However, in a recent study (26), pathological examination illustrated that silica nanoparticles possess good tissue biocompatibility after oral and intravenous injection, suggesting that these modes of administration are likely the safest routes to utilize during biomedical application.

We have synthesized and characterized liposome encapsulated mesoporous silica core shell magnetic iron oxide nanoparticles (i.e., Lipo[MNP@m-SiO$_2$]). Integration of organic dye into the Lipo[MNP@m-SiO$_2$] allowed us to observe the drug delivery system using MR and fluorescent imaging techniques: this dual modal imaging (MR and fluorescent nanoparticles) combines the enriched anatomical information obtained with MRI with the more detailed subcellular information collected with fluorescence imaging (27). Dual-modality MR and fluorescence imaging also allows for more specific information to be accessed vis-à-vis the targeted cell type or tissue. For example, the application of dual MR and fluorescent nanoprobe imaging has been investigated for primary draining or sentinel lymph nodes (28). The synthesis of similar nanoparticles for dual modal imaging has also been reported by various other studies (27, 29, 30). Unlike these previous studies, however, we selected biocompatible silica material for the surface of the organic dye-incorporated MNPs and then coated this surface with liposomes, enabling us to make modifications in order to target specific sites using ligand conjugation. Moreover, the incorporation of organic dye into the MNP itself indicates that other small drugs could also be integrated and delivered during disease therapy.

Lipo[MNP@m-SiO$_2$] has multiple functions that can be utilized for simultaneous multimodal imaging and therapy: as a targeted nanosystem, it can deliver drugs in a passive or active manner. Passive drug delivery takes advantage of the poor lymphatic system and leaky vasculature of tumor tissues (otherwise known as the "enhanced permeability and retention" effect) (31, 32), which allows for enhanced deposition of delivery nanoparticles at the site of solid tumors. In contrast, active drug delivery is performed via covalent conjugation of targeting molecules on the nanoparticle surface, which can recognize and bind to specific ligands expressed specifically in cancer cells.

In the present study, we showed specific binding of

Lipo[MNP@m-SiO$_2$]-Her2$_{Ab}$ to Her2/neu-overexpressing breast cancer cells, suggesting that this delivery system could potentially be applied in breast cancer treatments using MRI monitoring. Trastuzumab was intended for use as a targeting ligand rather than as a therapeutic agent; thus, the concentration used in the study was far below its potential therapeutic dose. Previous studies have shown that the combination of trastuzumab with conventional chemotherapy leads to increased response rates (33, 34).

However, it should also be noted that specifically targeting a contrast agent to the desired area can result in a lower required dosage to obtain a diagnostic response. We investigated this phenomenon for the trastuzumab-conjugated Lipo[MNP@m-SiO$_2$] by tracking these particles after being introduced to Her2/neu-overexpressing breast cancer cells using a fluorescence confocal microscope and in $vitro$ MR imaging. Our results suggest: trastuzumab-conjugated nanoparticles accumulate in detectable amounts in tumors expressing the Her2/neu receptor. Thus, we hypothesize that using this system would allow for lower levels of an MNP-integrated drug to be utilized during treatment as the majority of it would be directly transferred into the Her2/neu-overexpressing cancer cell. Future work will ideally incorporate other small drugs or dyes into the MNP of this this system and utilize multimodal imaging to monitor their uptake and therapeutic effects.

In conclusion, we have synthesized and characterized a liposome-coated silica core shell fluorescent MNP (i.e., Lipo[MNP@m-SiO$_2$]) delivery system and have identified the appropriate in $vitro$ multimodal imaging techniques and drug loading capability of this system. It appears that trastuzumab-conjugated Lipo[MNP@m-SiO$_2$] may be a potential tool for targeted drug delivery in Her2/neu-positive breast cancer cases.

REFERENCES

1. Atri M. New technologies and directed agents for applications of cancer imaging. *J Clin Oncol* 2006;24:3299-3308
2. Funovics MA, Kapeller B, Hoeller C, Su HS, Kunstfeld R, Puig S, et al. MR imaging of the her2/neu and 9.2.27 tumor antigens using immunospecific contrast agents. *Magn Reson Imaging* 2004;22:843-850
3. Rogers WJ, Basu P. Factors regulating macrophage endocytosis of nanoparticles: implications for targeted magnetic resonance plaque imaging. *Atherosclerosis* 2005;178:67-73
4. Gupta AK, Gupta M. Synthesis and surface engineering of iron oxide nanoparticles for biomedical applications. *Biomaterials* 2005;26:3995-4021

5. Schellenberger E, Schnorr J, Reutelingsperger C, Ungethüm L, Meyer W, Taupitz M, et al. Linking proteins with anionic nanoparticles via protamine: ultrasmall protein-coupled probes for magnetic resonance imaging of apoptosis. *Small* 2008;4:225-230

6. Li Z, Tan B, Allix M, Cooper AI, Rosseinsky MJ. Direct coprecipitation route to monodisperse dual-functionalized magnetic iron oxide nanocrystals without size selection. *Small* 2008;4:231-239

7. Kim J, Kim HS, Lee N, Kim T, Kim H, Yu T, et al. Multifunctional uniform nanoparticles composed of a magnetite nanocrystal core and a mesoporous silica shell for magnetic resonance and fluorescence imaging and for drug delivery. *Angew Chem Int Ed Engl* 2008;47:8438-8441

8. Slowing II, Vivero-Escoto JL, Wu CW, Lin VS. Mesoporous silica nanoparticles as controlled release drug delivery and gene transfection carriers. *Adv Drug Deliv Rev* 2008;60:1278-1288

9. Cao H, Gan J, Wang S, Xuan S, Wu Q, Li C, et al. Novel silica-coated iron-carbon composite particles and their targeting effect as a drug carrier. *J Biomed Mater Res A* 2008;86:671-677

10. Kim T, Momin E, Choi J, Yuan K, Zaidi H, Kim J, et al. Mesoporous silica-coated hollow manganese oxide nanoparticles as positive T1 contrast agents for labeling and MRI tracking of adipose-derived mesenchymal stem cells. *J Am Chem Soc* 2011;133:2955-2961

11. Yoon TJ, Kim JS, Kim BG, Yu KN, Cho MH, Lee JK. Multifunctional nanoparticles possessing a "magnetic motor effect" for drug or gene delivery. *Angew Chem Int Ed Engl* 2005;44:1068-1071

12. Sun C, Lee JS, Zhang M. Magnetic nanoparticles in MR imaging and drug delivery. *Adv Drug Deliv Rev* 2008;60:1252-1265

13. Olayioye MA. Update on HER-2 as a target for cancer therapy: intracellular signaling pathways of ErbB2/HER-2 and family members. *Breast Cancer Res* 2001;3:385-389

14. Slamon DJ, Godolphin W, Jones LA, Holt JA, Wong SG, Keith DE, et al. Studies of the HER-2/neu proto-oncogene in human breast and ovarian cancer. *Science* 1989;244:707-712

15. Chen TJ, Cheng TH, Chen CY, Hsu SC, Cheng TL, Liu GC, et al. Targeted Herceptin-dextran iron oxide nanoparticles for noninvasive imaging of HER2/neu receptors using MRI. *J Biol Inorg Chem* 2009;14:253-260

16. Hilger I, Leistner Y, Berndt A, Fritsche C, Haas KM, Kosmehl H, et al. Near-infrared fluorescence imaging of HER-2 protein over-expression in tumour cells. *Eur Radiol* 2004;14:1124-1129

17. Tran TA, Ekblad T, Orlova A, Sandström M, Feldwisch J, Wennborg A, et al. Effects of lysine-containing mercaptoacetyl-based chelators on the biodistribution of 99mTc-labeled anti-HER2 Affibody molecules. *Bioconjug Chem* 2008;19:2568-2576

18. Lee H, Yoon TJ, Figueiredo JL, Swirski FK, Weissleder R. Rapid detection and profiling of cancer cells in fine-needle aspirates. *Proc Natl Acad Sci U S A* 2009;106:12459-12464

19. Stanisic DI, Martin LB, Liu XQ, Jackson D, Cooper J, Good MF. Analysis of immunological nonresponsiveness to the 19-kilodalton fragment of merozoite surface Protein 1 of Plasmodium yoelii: rescue by chemical conjugation to diphtheria toxoid (DT) and enhancement of immunogenicity by prior DT vaccination. *Infect Immun* 2003;71:5700-5713

20. Kim JS, Yoon TJ, Yu KN, Noh MS, Woo M, Kim BG, et al. Cellular uptake of magnetic nanoparticle is mediated through energy-dependent endocytosis in A549 cells. *J Vet Sci* 2006;7:321-326

21. Jain TK, Richey J, Strand M, Leslie-Pelecky DL, Flask CA, Labhasetwar V. Magnetic nanoparticles with dual functional properties: drug delivery and magnetic resonance imaging. *Biomaterials* 2008;29:4012-4021

22. Cheng HL, Stikov N, Ghugre NR, Wright GA. Practical medical applications of quantitative MR relaxometry. *J Magn Reson Imaging* 2012;36:805-824

23. Lee JE, Lee N, Kim T, Kim J, Hyeon T. Multifunctional mesoporous silica nanocomposite nanoparticles for theranostic applications. *Acc Chem Res* 2011;44:893-902

24. Casciaro S, Conversano F, Ragusa A, Malvindi MA, Franchini R, Greco A, et al. Optimal enhancement configuration of silica nanoparticles for ultrasound imaging and automatic detection at conventional diagnostic frequencies. *Invest Radiol* 2010;45:715-724

25. Napierska D, Thomassen LC, Rabolli V, Lison D, Gonzalez L, Kirsch-Volders M, et al. Size-dependent cytotoxicity of monodisperse silica nanoparticles in human endothelial cells. *Small* 2009;5:846-853

26. Fu C, Liu T, Li L, Liu H, Chen D, Tang F. The absorption, distribution, excretion and toxicity of mesoporous silica nanoparticles in mice following different exposure routes. *Biomaterials* 2013;34:2565-2575

27. Sung CK, Hong KA, Lin S, Lee Y, Cha J, Lee JK, et al. Dual-modal nanoprobes for imaging of mesenchymal stem cell transplant by MRI and fluorescence imaging. *Korean J Radiol* 2009;10:613-622

28. Bumb A, Regino CA, Egen JG, Bernardo M, Dobson PJ, Germain RN, et al. Trafficking of a dual-modality magnetic resonance and fluorescence imaging superparamagnetic iron oxide-based nanoprobe to lymph nodes. *Mol Imaging Biol* 2011;13:1163-1172

29. Lu CW, Hung Y, Hsiao JK, Yao M, Chung TH, Lin YS, et al. Bifunctional magnetic silica nanoparticles for highly efficient human stem cell labeling. *Nano Lett* 2007;7:149-154

30. Veiseh O, Sun C, Gunn J, Kohler N, Gabikian P, Lee D, et al. Optical and MRI multifunctional nanoprobe for targeting gliomas. *Nano Lett* 2005;5:1003-1008

31. Maeda H, Wu J, Sawa T, Matsumura Y, Hori K. Tumor vascular permeability and the EPR effect in macromolecular therapeutics: a review. *J Control Release* 2000;65:271-284

32. Noguchi Y, Wu J, Duncan R, Strohalm J, Ulbrich K, Akaike T, et al. Early phase tumor accumulation of macromolecules: a great difference in clearance rate between tumor and normal

tissues. *Jpn J Cancer Res* 1998;89:307-314

33. Merlin JL, Barberi-Heyob M, Bachmann N. In vitro comparative evaluation of trastuzumab (Herceptin) combined with paclitaxel (Taxol) or docetaxel (Taxotere) in HER2-expressing human breast cancer cell lines. *Ann Oncol*

2002;13:1743-1748

34. Pegram MD, Konecny GE, O'Callaghan C, Beryt M, Pietras R, Slamon DJ. Rational combinations of trastuzumab with chemotherapeutic drugs used in the treatment of breast cancer. *J Natl Cancer Inst* 2004;96:739-749